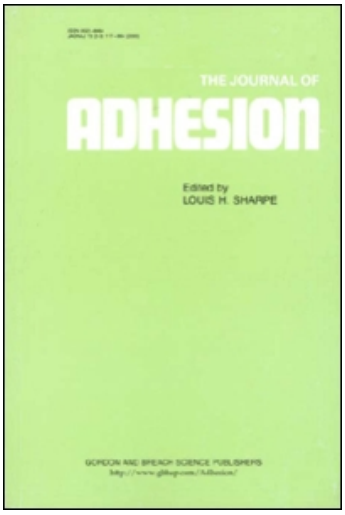

The Journal of Adhesion
Publication details, including instructions for authors and subscription information:
http://www.informaworld.com/smpp/title~content=t713453635

Thermodynamics of a Stable Blister Delamination at Elevated Temperature

Kai-Tak Wan[a]; Christopher D. Breach[a]
[a] Process Technology Division, Gintic Institute of Manufacturing Technology, Singapore

To cite this Article Wan, Kai-Tak and Breach, Christopher D.(1998) 'Thermodynamics of a Stable Blister Delamination at Elevated Temperature', The Journal of Adhesion, 66: 1, 183 — 202
To link to this Article: DOI: 10.1080/00218469808009965
URL: http://dx.doi.org/10.1080/00218469808009965

J. Adhesion, 1998, Vol. 66, pp. 183–202
Reprints available directly from the publisher
Photocopying permitted by license only

Thermodynamics of a Stable Blister Delamination at Elevated Temperature

KAI-TAK WAN* and CHRISTOPHER D. BREACH

Process Technology Division, Gintic Institute of Manufacturing Technology, 71 Nanyang Drive, Singapore 638075

(Received 23 July 1997; In final form 29 September 1997)

A new blister test using thermal expansion of an internal working gas trapped at a dissimilar interface between a thin polymer coating and a rigid adherend is developed to measure the adhesive strength at elevated temperature. The blister dimensions are measured by a thermomechanical analyser (*TMA*) and an optical microscope as a function of temperature. The thermodynamics is presented based on both linear elastic fracture mechanics and the ideal gas law.

Keywords: Blister test; adhesion; *TMA*; fracture mechanics; delamination

INTRODUCTION

The adhesion of thin polymer coatings on rigid substrates is important in the electronics industry. Weak adhesion strength causes delamination and premature failure of parts. The predominant failure mode in industry is due to the thermal expansion of air and/or moisture trapped at the many interfaces and the subsequent debonding [1]. To understand the basic adhesion mechanism, a range of adhesion tests with different geometries have been devised and well documented, such as the peel test and double cantilever. However, severe plastic deformation occurring in most conventional methods tends to obscure

*Corresponding author.

the adhesion energy which is the critical material/interface parameter to thin film delamination [2, 3]. Another problem is that most test geometries do not resemble the common failure modes.

To minimise plastic energy, the blister test is by far the most promising because of the low peeling angle, the axial symmetry of delamination, and the uniform pressure loading without a mechanical fixture [4–11]. However, the method is notoriously restricted by its instability at crack initiation [4]. The strain energy releases rate, G, takes the form of $G \propto p^2 a^4$ [4] for pure bending and $G \propto p^4 a^4$ [6] for pure stretching, where p is the uniform applied pressure and a the blister radius. In either case, the blister crack grows in a catastrophic manner once the pressure exceeds a threshold.

Complicated computer interfaces constructed with differential pressure sensors and regulators are, therefore, necessary to monitor the applied pressure and delamination area simultaneously [9]. Ingenious methods of island [12–13] and peninsular [14] blisters were developed recently and successfully "stabilised" the otherwise unstable crack propagation, though both are restricted by the complications in sample preparation and fracture analysis. Another method is the constrained blister [15–17] which retains the axisymmetric blister geometry by placing a flat constraint above the blister to limit the vertical displacement and achieves a nearly constant G. One disadvantage, however, is that the specimen size has to be in the range of tens of millimeters, since there is a minimum distance the constraining plate can be located above the substrate. The method, being excellent in investigating structural adhesive in large specimens, is not appropriate in small electronics parts.

A new approach to ensure a *stable* crack propagation in a conventional blister geometry is due to the expansion of an internal "working gas" [18]. In this method, a fixed amount of gas is deliberately trapped at the membrane/substrate interface before exposing the specimen to a reduced external pressure. The pressure gradient drives a blister delamination into the dissimilar interface. Meanwhile, the blister volume expands and the internal pressure decreases following the ideal gas law. Thus, the crack driving force (G) diminishes as the blister grows. Such a natural feedback mechanism stabilises the debonding process. The method is applicable to specimens of any size. In order to simulate further the industrial

failure mode of delamination at high temperature, thermal expansion of the working gas is employed as a crack driving force in this paper. We will show that the debonding process remains stable.

The simple linear elastic fracture analysis in our previous work [18] is now complicated by a long list of details such as

(i) The thermal viscoelastic mechanical properties of the polymer, *e.g.*, elastic modulus and apparent film thickness,
(ii) Residual stress due to thermal mismatch,
(iii) Thermal expansion of film which changes the blister geometry,
(iv) Temperature dependence of interfacial chemistry as manifested by the adhesive strength, and
(v) Sublimation/evaporation of volatile impurities (*e.g.*, water droplets) within the blister void at some critical temperature, etc.

To address every physical and chemical issue lies beyond the scope of this paper, though the industrial relevance justifies such an effort in the long run. In this paper, we will construct a simple model based on linear elastic fracture mechanics (LEFM), the ideal gas law, and an assumption that only the thermal dependence of elastic modulus of the film is of significance. We will show how the theory fits the experimental data semi-quantitatively.

A STABLE BLISTER TEST

Figure 1 shows a thin polymer film adhered to a rigid substrate with a blind hole of radius a_0. Upon heating, the fixed mass of working gas expands and drives a blister delamination. A thermomechanical analyser (*TMA*) probe under a known external load, F, pressing against the bulging blister records the height, y_0, as a function of temperature, T. Since most *TMA* measurements require a small but finite F to avoid vibration of the probe, a contact area, πc^2, is inevitable. The resulting geometry resembles that of a "constrained blister" [15], though the constraining plate, *i.e.*, the *TMA* probe, is now allowed a free vertical movement. At low temperatures, the blister height is negligibly small compared with the lateral radius, the contact area is large and the blister resembles a "flat disc". As temperature

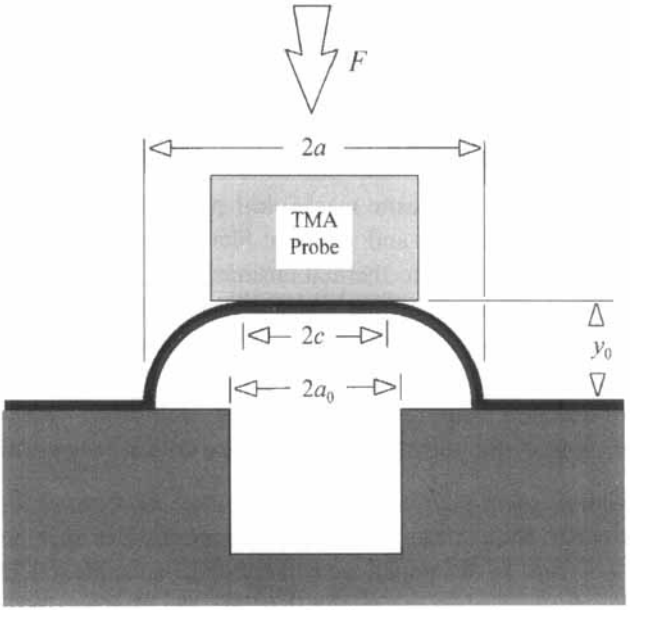

FIGURE 1 Sketch of a blister delamination along the polymer/substrate interface. The crack was driven by an expanding internal gas trapped in a dead volume drilled in the substrate. A *TMA* probe under an external load, F, was to measure the blister height, y_0, as a function of temperature. The bore radius (a_0), blister radius (a), and contact radius (c) are shown.

increases, the membrane curvature increases and the blister eventually becomes spherical at high internal pressure.

In this paper, we will derive the analytical fracture equations in the case of a vanishing F by modifying our previous model for stable blister crack [18], and will expand to the case of a finite F. It will soon become obvious that the $F=0$ limit is good in its simplicity and clarity, yet fails to account for the onset of blister bulging.

We being by establishing the elasticity equations of a conventional blister test under a uniform constant pressure, p. For a thin circular plate of radius a (and debonding area $A=\pi a^2$), thickness h, elastic modulus E and Poisson ratio ν, being stretched without bending, the blister geometry according to Hencky is given by [19]

$$y(r) = \left(\frac{pa^4}{Eh}\right)^{1/3} \sum_{i=0} \lambda_{2i} \left[1 - \left(\frac{r}{a}\right)^{2i+2}\right] \tag{1}$$

and the central deflection or blister height

$$y_0 = C_2\left(\frac{pa^4}{Eh}\right)^{1/3} = C_2\left(\frac{pA^2}{\pi^2 Eh}\right)^{1/3} \tag{2}$$

where $C_2 = \sum_{i=0} \lambda_{2i}$ with λ_i being some numerical constants. The blister volume is given by

$$V = \int_0^a 2\pi r y(r) dr = C_1 A y_0 \tag{3}$$

where

$$C_1 = 1 - \frac{1}{C_2}\sum_{i=0} \frac{\lambda_{2i}}{i+2}.$$

As reported by a number of authors, a number of numerical mistakes were found in Hencky's paper [6]. We compute the geometrical constants C_1 and C_2 to be $C_1(\nu = 0.3) = 0.521$ and $C_1(\nu = 0.5) = 0.516$, and $C_2(\nu = 0.3) = 0.654$ and C_2 ($\nu = 0.5$) $= 0.595$. In a spherical blister approximation [8], $C_1 = 1/2$ and $C_2 = [(1 - \nu)/2]^{1/3}$. Eqs. (1) to (3) are valid in the case where the *TMA* probe exerts a zero force on the blister. Note that E is a function of T.

Next we consider a fixed amount of working gas. Heating of the internal gas first leads to a blister bulging in a pre-delamination stage, followed by debonding along the dissimilar interface. The process is governed by the isothermal ideal gas law:

$$(p + p_0)(V + V_0) = nRT \tag{4}$$

or

$$\left(1 + \frac{p}{p_0}\right)\left(1 + \frac{V}{V_0}\right) = \frac{T}{T_0} \tag{4a}$$

with p_0 the atmospheric pressure, V_0 the dead volume under the membrane (see Fig. 1), n the mass of working gas available in moles, R the gas constant, T the absolute temperature and T_0 the room

temperature defined as $T_0 = p_0 V_0/nR$. We will compile the result for: (a) $p_0 \neq 0$ and $V_0 \neq 0$, and (b) $p_0 = 0$ and $V_0 = 0$ which is a limiting case. The assumptions in case (b) correspond to a practical situation where water is trapped at a flat interface ($V_0 = 0$) and evaporates and expands under an increasing temperature in a vacuum environment ($p_0 = 0$).

The thermodynamics of a quasi-static delamination process is shown in Figure 2. Beginning at point A at room temperature T_0, heating of the sample to $T = (T_0 + \Delta T)$ leads to a blister expansion in the vertical direction quasi-statically *without* interfacial debonding (*i.e.*, A remains unchanged and $a = a_0$) reaching point B. In this pre-

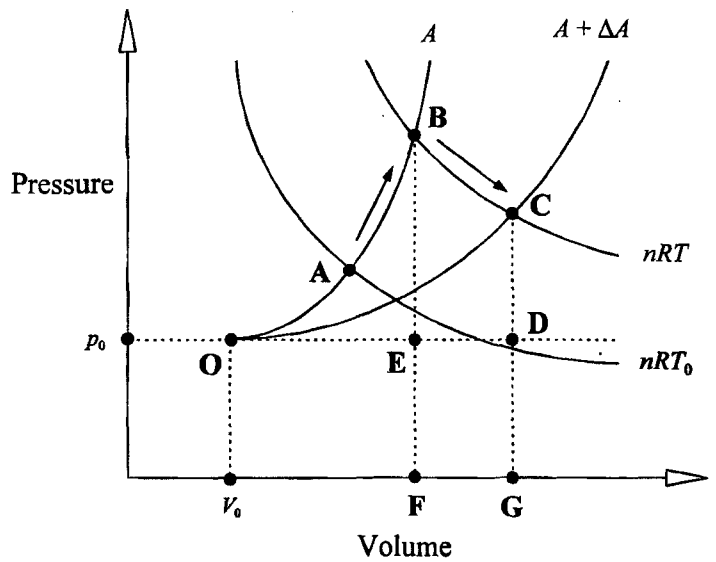

FIGURE 2 The p-V relationship for a blister with fixed amount of working gas. Point O represents the ambient conditions (p_0, V_0, T) in which the specimen is prepared. Curve OAB denotes the behaviour for a fixed debonded area A, and curve OC for $(A + \Delta A)$, both following Eq. (5). Two other curves are drawn to show the ideal gas law: $(p + p_0)(V + V_0) = nRT_0$ (passing through point A) and $(p + p_0 + \Delta p)$ $(V + V_0 + \Delta V)$ = nRT (curve BC). Point A is at equilibrium with n moles of working gas at temperature T_0, while points B and C are at T. When temperature increases from T_0 to T, blistering occurs without debonding and follows a path from points A to B. The excess pressure at B drives a delamination along path BC isothermally before reaching point C where equilibrium is attained. In path BC, changes in potential and elastic energy are shown as dU_P = area $BCGF$ (or $BCDE$ when $p_0 = 0$ and $V_0 = 0$) and $dU_E = \Delta OCD - \Delta OBE$, respectively.

delamination stage, the blister geometry is governed by Eqs. (2), (3) and (4) such that

$$\frac{\Delta T}{T_0}=\left(\frac{C_1 Eh}{C_3^2 a_0^2 p_0 V_0}\right)y_0^4+\left(\frac{Eh}{C_2^3 a_0^2 p_0}\right)y_0^3+\left(\frac{C_1\pi a_0^2}{V_0}\right)y_0 \quad \text{for case (a)} \qquad (5a)$$

$$y_0=\left(\frac{C_2^3 a_0^2}{\pi^2 C_1 Eh}\right)^{1/4}(nRT)^{1/4} \quad \text{for case (b).} \qquad (5b)$$

It is interesting to remark that Eq. (5a) can be re-written as $y_0 = y_0(T)$, and that $y_0(\Delta T=0)=0$ in Eq. (5a) and $y_0(T=0)=0$ in Eq. 5(b). Blistering always prevails at any temperature in case (b) because $p=0$ and $V=0$ only at $T=0$. Along path AB, the increases in potential energy, U_P, of the working gas and elastic energy, U_E, in the film are simply absorbed from the surrounding reservoir. Since there is no fracture process along this path, ΔU_P and ΔU_E do *not* contribute to the strain energy release rate, G.

At point B, where excess internal pressure is acting on the membrane, the blister crack begins to grow spontaneously and isothermally reaching point C where equilibrium is finally established. Along the path BC, the debonding area changes from A to $(A+\Delta A)$, blister height from y_0 to $(y_0+\Delta y_0)$, blister volume from V to $(V+\Delta V)$, and internal pressure from (p_0+p) to $(p_0+p+\Delta p)$, where ΔA, Δy_0 and ΔV are positively defined and Δp is negative. Neglecting any kinetic energy, the strain energy release rate, G, is defined as [20]

$$G=\frac{d}{dA}(U_P-U_E) \qquad (6)$$

so that $G=W$, the interface energy, at equilibrium. Note that U_P has an intrinsic energy dissipation component because of the isothermal, rather than adiabatic, process governed by the ideal gas law. Thus, the fracture process, though elastic, is irreversible. The increment of external work done from B to C is given by the area $BCGF$ in case (a) and $BCDE$ in case (b):

$$dU_P=\int_{BC} p+p_0\,dV$$

$$\approx \frac{nRT}{V+V_0}dV \qquad \text{for case (a)} \qquad (7a)$$

$$\approx \frac{nRT}{V}dV \qquad \text{for case (b).} \qquad (7b)$$

Note that points D and E coincide with G and F, respectively, when $p_0 = 0$. The elastic energy stored in a blister is found to be [6]

$$U_E = \int p(V)dV|_A = \frac{pV}{4} \tag{8}$$

which is represented by the area ΔOBE for configuration B and ΔOCD for C. In case (b), $U_E = pV/4 = nRT/4$, so $dU_E = 0$ and the new debonding surface is created at the expense of U_P only. Substituting Eqs. (7) and (8) into (6),

$$\mathcal{G} = -\frac{nRT}{V_0 + V}\left(\frac{dV}{dA}\right) - \left[\frac{p}{4}\left(\frac{dV}{dA}\right) + \frac{V}{4}\left(\frac{dp}{dA}\right)\right] \quad \text{for case (a)} \tag{9a}$$

$$G = \frac{nRT}{V}\left(\frac{dV}{dA}\right) \quad \text{for case (b)} \tag{9b}$$

(cf. $G = p\,(dV/dA)$ in the case of a blister under constant pressure with negligible elastic energy). At point C, equilibrium prevails, $G = W$, and substituting Eq. (3) into (9),

$$W = \frac{5pV}{4A} f(p, V, p_0, V_0) \quad \text{for case (a)} \tag{10a}$$

$$W = \frac{5pV}{4A} = \frac{5}{4}\left(\frac{nRT}{A}\right) \quad \text{for case (b)} \tag{10b}$$

where

$$f(p, V, p_0, V_0) = 1 + \frac{4(p_0 V + p_0 V_0)}{4pV + 3pV_0 + p_0 V}.$$

In the case of $p_0 = 0$ and $V_0 = 0$, $f(p, V, 0, 0) = 1$ and Eq. (10a) reduces to Eq. (10b). It is interesting to note that $G = (5\,pV/4A)$ for a blister delamination under constant pressure [6, 18]. The dimensionless function $f(p, V, p_0, V_0)$ describes the thermal expansion of the working gas. It can be shown that $(dG/dA) < 0$ in both Eqs. (10a) and (10b), and the fracture process is stable. If a blister, after some delamination at an elevated temperature, is now cooled to ambient, $y_0(T)$ in the "unloading" process will be governed by Eq. (5) with a_0 replaced by the new blister radius a.

Thermal Expansion of Working Gas Under Finite *TMA* Probe Force ($F \neq 0$)

In the case of a finite F, the probe's is supported by air pressure *via* the content area πc^2. Therefore,

$$F = \pi c^2 p \tag{11}$$

There are a few interesting features in Eq. (11). Firstly, at high T, p is large and c tends to zero. The effect of a finite F, therefore, becomes minimal and the blister mechanics reduces to that $F=0$ as in the previous section. Secondly, Eq. (11) is valid only for $c \geq a_0$. When p increases to a critical value, p^*, with

$$p^* = \frac{F}{\pi a_0^2}, \tag{12}$$

the *TMA* weight is lifted and blistering follows. This happens when the temperature reaches

$$T^* = T_0\left(1 + \frac{F}{\pi a_0^2 p_0}\right) \tag{13}$$

by substituting Eq. (12) into (4b). For $T < T^*$, the *TMA* probe is in contact with the substrate (*via* the film) and $V=0$. The measured $y_0(T)$ is, therefore, expected to be the sum of the thermal expansions of the substrate and the through-thickness expansion of the film (with the latter being negligibly small), independent of all material parameters of the film (E and h) and the interface (W). When $F=0$, T^* reduces to T_0, *i.e.*, blistering occurs once heating begins (cf. Eq. (5a)).

Analytical solutions for the constrained blister are readily available from Dillard *et al.* [15–17], and independently from Williams [21], yet the blister is confined to a maximum vertical displacement in either case. We will modify Williams' model to accommodate a variable blister height and introduce thermal expansion of the working gas as the crack-driving force. Based upon an average stress and strain approximation [20], Williams deduced that for a blister under uniform pressure, p, and a constant y_0, the blister geometry and the strain

energy release rate are given by

$$y = \frac{pa^2}{4\sigma h}\left[1 - \frac{r^2}{a^2} + 2\frac{c^2}{a^2}\ln\left(\frac{r}{a}\right)\right] \quad \text{for } a \geq r \geq c$$

$$y = y_0 = \frac{pa^2}{4\sigma h}\left[1 - \zeta^2 + \zeta^2 \ln \zeta^2\right] \quad \text{for } r < c \tag{14}$$

where $\zeta = c^2/a^2$ and the radial stress σ defined as

$$\sigma^3 = \frac{Ep^2a^2}{32h^2}\left[1 - 3\zeta^2 + \frac{2\zeta^4}{1-\zeta^2}\ln\frac{1}{\zeta^2}\right]; \tag{15}$$

and

$$G = \frac{5py_0}{8} g_0(\zeta) \tag{16}$$

where

$$g_0(\zeta) = \frac{5 - 16\zeta^2 + 15\zeta^4 - 4\zeta^6 - 2\zeta^4 \ln \zeta^2}{5(1-\zeta^2)(1 - \zeta^2 + \zeta^2 \ln \zeta^2)}$$

respectively [21]. Williams added an extra term $G_c = -(\sigma\, h\, \varepsilon)$ to G in Eq. (16), with ε the elastic strain, to account for the increase in contact area, πc^2, as the delamination propagates. This term is ignored in this work, since πc^2 is ever diminishing while the blister crack propagates and the TMA probe move upwards. Note that when $\zeta = 0$, Eq. (14) reduces to $y_0 = (1/2)\,(pa^4/Eh)^{1/3}$ (*i.e.*, $C_2 = 1/2$ in Eq. (2)) which differs from Hencky's solution only by a numerical constant, a consequence of the spherical geometry assumed by Williams.

For a variable y_0, Eqs. (14) and (15) remain valid. The constrained blister volume is found by integrating $y(r)$ (Eq. (14)):

$$V = \int_0^a 2\pi r y(r) dr + \pi c^2 y_0 = \frac{1}{2} A y_0\, \nu(\zeta) \tag{17}$$

where the dimensionless function $\nu(\zeta)$ is defined as

$$\nu(\zeta) = \frac{(1-\zeta^2)^2}{1 - \zeta^2 + \zeta^2 \ln \zeta^2}.$$

When $F = 0$, $\nu(0) = 1$ and Eq. (17) reduces to $V = Ay_0/2$ (*i.e.*, in Eq. (3)).

Since y_0 is treated as a variable in this paper, an extra term to account for the potential energy gained by the TMA weight must be subtracted from the energy balance:

$$\frac{dU_{TMA}}{dA} = \frac{d(Fy_0)}{dA}\bigg|_p = py_0\left[\frac{\zeta^2(1-\zeta^2)}{1-\zeta^2+\zeta^2\ln\zeta^2}\right] \tag{18}$$

which vanishes when $c=0$ or $F=0$. The mechanical energy release rate thus becomes:

$$G \approx \frac{5py_0}{8} g_0(\zeta) f(p, V, p_0, V_0) - \frac{dU_{TMA}}{dA} \tag{19a}$$

$$\approx \frac{5pV}{4A} g_1(\zeta) f(p, V, p_0, V_0) - \frac{dU_{TMA}}{dA} \tag{19b}$$

where $g_1(\zeta)=g_0(\zeta)/\nu(\zeta)$. The dimensionless function $f(p, V, p_0, V_0)$ again accounts for the differential energy changes of the working gas. When $F=0$, $g_0(0)=g_2(0)=1$ and Eq. (19) reduce to $G=[(5/8)\, py_0]=(5pV/4A)$ (cf. Eqs. (10a) and (10b)). A more detailed calculation will be published elsewhere [22].

EXPERIMENTAL METHODS

As noted earlier, the thermal properties of the coating-interface-substrate systems pose serious difficulties in a quantitative analysis. The experiments described below are aimed at illustrating the theory in a semi-quantitative manner. A commercially-available masking tape was chosen as the polymer film and aluminium as the substrate because of the case of specimen preparation. Differential Scanning Calorimetry (DSC) measurements on the polymeric film revealed that melting occurred at $T>150$°C. The temperature dependence of elastic modulus and the phase angle were measured by a Dynamic Mechanical Thermo Analyser (DMTA) as shown in Figure 3.

Three aluminium cylinders with a 10 mm diameter were mechanically drilled along the axis to make blind holes with dimensions (1) $\phi 2$ mm, height 9.995 mm, depth 7.414 ± 0.123 mm and $V_0 \approx 22.03 \pm 0.39$ mm^3 (taking into account the drill geometry); (2) $\phi 3$ mm, height 8.643 mm,

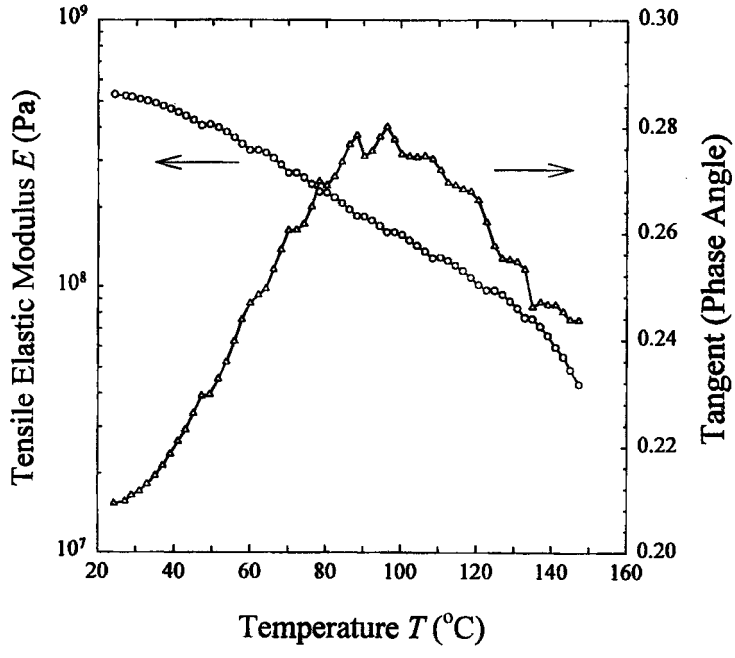

FIGURE 3 Elastic modulus (circles) and tangent phase angle (triangles) of a stack of 10 layers of masking tape as a function of temperature using a DMTA. The specimen, with an overall thickness of 510 μm, width 10 mm, effective length 20 mm, experienced cyclic loading of a peak-to-peak displacement of ±16 mm and frequency 1 Hz. Heating rate was 5°C. min^{-1}. Serious melting occurred at temperature above 150°C.

depth 3.245±0078 mm and $V_0 \approx 18.69 \pm 0.55$ mm^3, and (3) ϕ4 mm, height 9.350 mm, depth 3.292±0.048 mm and $V_0 \approx 31.30 \pm 0.60$ mm^3. The surface was then polished to 3 μm, acetone cleaned and dried thoroughly. A polymer film with a thickness of 50 μm was then adhered onto the polished surface, sealing a known volume of air in the hermetic bore. Two experiments were run in parallel to measure the lateral blister dimension ($2a$) and the vertical dimension (y_0) as a function of T.

In the first experiment, specimens were immersed in water for 30 seconds at a desired temperature. The blister diameter was then measured post-mortem using an optical microscope. In this case, there was no external force pressing on the blister. In a second experiment, a Dupont *TMA* probe with a small force in the range of 0.01 to 0.15 N was put directly above the bore *via* the memberane to measure the

blister height (Fig. 1), when the temperature was scanned from ambient (25°C) to a desired temperature (below 150°C) and back to room temperature at a rate of ±3°C min^{-1}. Our experiments showed that a higher heating rate resulted in differential heating, making the working gas cooler than the bulk aluminium surroundings and, thus, a higher T^* than expected. A heating rate of 3°C. min^{-1} or below yielded consistent results.

RESULTS AND ANALYSIS

Figure 4 shows the blister diameter $2a$ as a function of temperature T, along with the best linear curve fits, measured after the specimens were

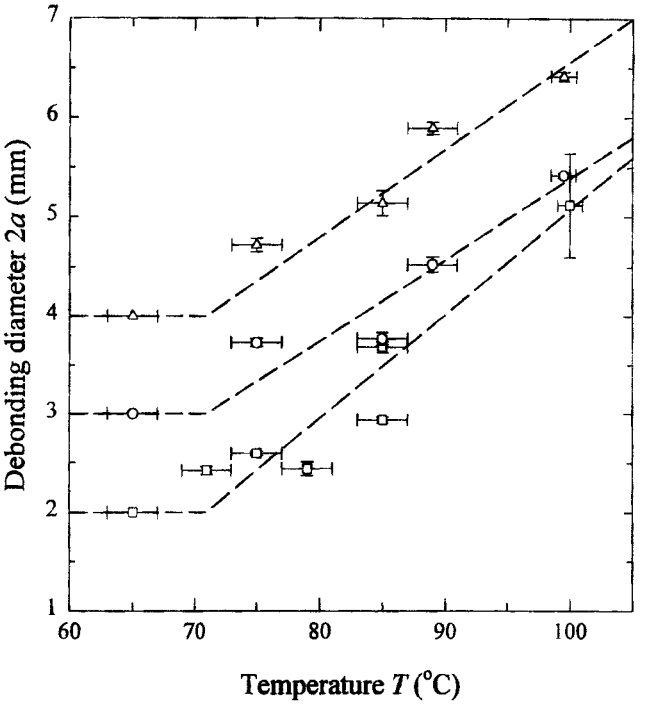

FIGURE 4 Blister diameter $2a$ of the specimens with $\phi 2$ mm bore (squares), $\phi 3$ mm bore (circles) and $\phi 4$ mm (triangles) after exposing specimens to warm water at temperature T for 30 seconds. Intercepts on the $2a$ axis are the bore diameter $2a_0$. Best linear curve fits are shown. No measurable delamination occurred at $T < 70$°C.

immersed in warm water. There was no observable delamination at $T < 70°C$. Debonding occurred thereafter as T increased.

Figures 5a to 5c show three typical *TMA* measurements. In Figure 5a, the speciment ($2a_0 = 3$ mm) was heated from 25°C to 110°C and cooled to 25°C under a *TMA* load of 0.05 N. The heating curve could be separated into 2 regions. From 30°C to 77°C, the slope of $y_0(T)$ represented $(20 \pm 1) \times 10^{-6} K^{-1}$ which coincided with the thermal expansion coefficient (CTE) of aluminium ($\alpha_{Al} = 25 \times 10^{-6} K^{-1}$). The

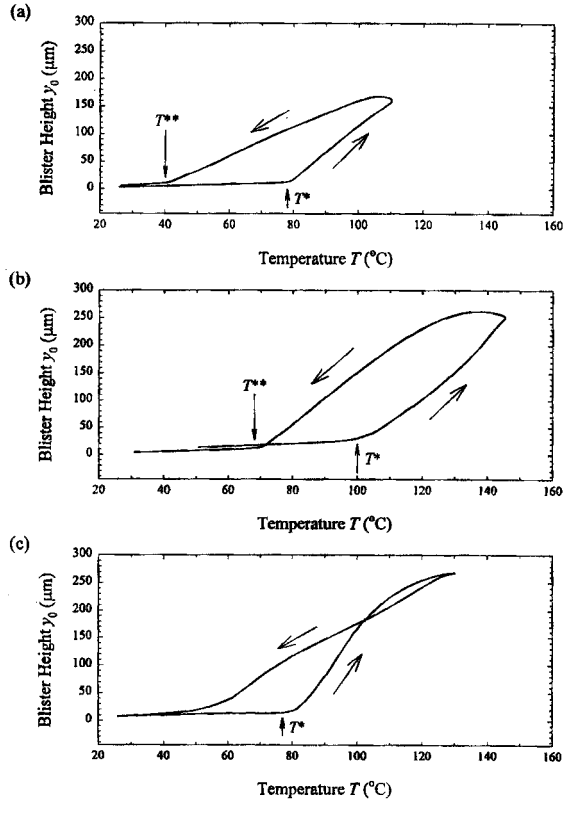

FIGURE 5 Typical $y_0(T)$ as measured by a *TMA* with a heating rate of 3°C. min^{-1} for an aluminium substrate with (a) $2a_0 = 3$ mm, $F = 0.05$N and substrate height 9.995 mm, (b) $2a_0 = 3$ mm, $F = 0.01$ N and substrate height 8.643 mm, (c) $2a_0 = 2$ mm, $F = 0.01$ N and substrate height 9.350 mm. The arrows denote the sequential heating (loading) and cooling (unloading). Temperature T^* marks the onset of lifting of *TMA* probe from substrate, and T^{**} the landing of the *TMA* probe on the substrate again.

probe was in contact with the substrate. There was a short transition around T^* of 77°C where blistering began, followed by debonding until the final temperature of 110°C was reached.

In the subsequent cooling or "unloading", y_0 reached a maximum of 168 μm at 106°C, then followed a different track according to Eq. (5a) with a constant blister radius attained at 110°C. The slope of $y_0(T)$ changed to 2.6 ± 0.2 μm·K^{-1}. A sharp change in (dy_0/dT) occurred at $T^{**} = 43$°C, when the blister finally collapsed and the *TMA* probe rested on the substrate again. The *TMA* measurement was expected to show the thermal contraction of aluminium hereafter. At $T < 43$°C, $y_0(T)$ represented $(40 \pm 3) \times 10^{-6}$K^{-1}(cf. α_{Al}). The discrepancy could be explained by a small permanent plastic deformation of the film acquired at high temperature. The post-mortem debonding diameter was measured to be $2a = 4.40 \pm 0.09$ mm by an optical microscope. It is interesting to note that the $2a$ can be predicted by the transition T^{**} Eq. (13) can be rearranged to

$$(T^* - T_0)(2a_0)^2 = (T^{**} - T_0)(2a)^2. \tag{20}$$

Substituting $T^* = 78 \pm 2$°C, $T^{**} = 43 \pm 2$°C, $T_0 = 25 \pm 2$°C and $2a_0 = 3 \pm 0.2$ mm into Eq. (20), $2a$ is calculated to be 5.14 ± 0.75 mm, which is reasonably close to the measured $2a$.

Figure 5b shows another *TMA* measurement with the same aluminium substrate and a new film. The *TMA* exerted a force of 0.01 N on the blister and the final temperature was 145°C. For $T < T^*$ ($= 100$°C), the slope of $y_0(T)$ represented $(24 \pm 2) \times 10^{-6}$ K^{-1} (cf. α_{Al}). Delamination took place from $T = 100$°C to 145°C. As the temperature dropped below $T^{**} = 67$°C in the cooling process, $y_0(T)$ represented $(28 \pm 2) \times 10^{-6}$ K^{-1} (cf. α_{Al}). Substituting $T^* = 100 \pm 2$°C, $T^{**} = 67 \pm 2$°C, $T_0 = 25 \pm 2$°C and $2a_0 = 3 \pm 0.2$ mm into Eq. (14), $2a$ was calculated to be 4.01 ± 0.60 mm, which was reasonably close to the measured $2a$ of 4.86 ± 0.01 mm. Figure 5c shows yet another *TMA* measurement with a different substrate with $2a_0 = 2$ mm and $F = 0.01$ N. Substituting the measured value of $2a = 5.28 \pm 0.06$ mm after the temperature scan into Eq. (2) showed that T^{**} falls below T_0. This explained the absence of a well defined T^{**} in Figure 5c.

A series of experiments was carried out to measure T^* at different F. In Figure 6, T^* is plotted as a function of $[F/(2a)^2]$ for substrates with

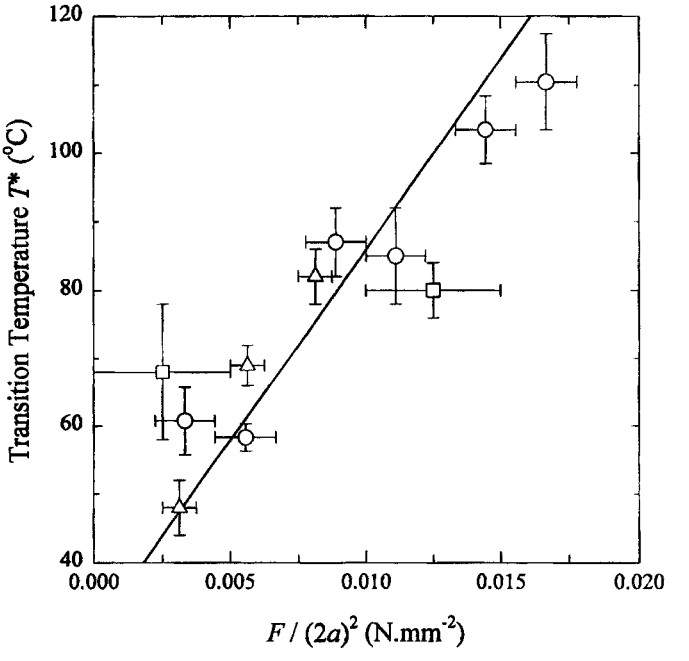

FIGURE 6 Transition temperature T^* when the weighted *TMA* probe was lifted from substrate as a function of $[F/(2a)^2]$ for specimens with a $\phi 2$ mm bore (squares), $\phi 3$ mm bore (circles) and $\phi 4$ mm (triangles). A best linear curve fit with $T_0 = 30°C$ is also shown.

bores of $\phi 2$ mm (squares), $\phi 3$ mm (circles) and $\phi 4$ mm (triangles). The error in F is taken to be 0.01 N. A linear graph according to Eq. (13) is shown with $T_0 = 30°C$ and a best fit slope of 5 ± 0.5 K·m^2·N^{-1} (cf. $4\,T_0/\pi p_0 \approx 3.8$ K·m^2·N^{-1} with $T_0 = 303$ K, $p_0 = 10^5$ Pa). The discrepancy is likely the consequence of (i) a long process zone behind the crack tip which gives rise to a larger apparent a_0 compared with the actual bore radius and (ii) the so far unacknowledged residual thermal stress.

We use Figures 5a to 5c as an illustration to calculate W from Eq. (19). Since the debonding radius could only be measured post-mortem, only G at maximum temperature was computed. In Figure 5a, $E = 128$ MPa (at 110°C from Fig. 3), $h = 50$ μm, $\nu = 0.3$, $2a = 4.40$ mm, $y_0 = 168$ μm, $F = 0.05$ N, $T = 110°C$, $p_0 = 10^5$ Pa, $V_0 = 18.9$ mm^3 and, thus, $p = 6520$ Pa, $V = 1.55$ mm^3 and $c = 0.70$ mm (from Eqs. (2), (3) and (11), respectively) and, therefore, $W = 13.4 \pm 2$ J·m^{-2} at 110°C.

Repeating the procedures for Figure 5b, $W = 19.8 \pm 2\ \mathrm{J \cdot m^{-2}}$ at 145°C. with $p = 0.0131$ MPa, $V = 3.24\ \mathrm{mm^3}$ and $c = 1.10$ mm; and for Figure 5c, $W = 16.0 \pm 2\mathrm{J \cdot m^{-2}}$ at 130°C with $p = 6530$ Pa, $V = 3.411\ \mathrm{mm^3}$ and $c = 0.70$ mm. (cf. $W = 35 \pm 4\ \mathrm{J \cdot m^{-2}}$ at 25°C measured for a similar interface [18]). Inconsistencies in W measured could possibly be due to thermal expansion of the film at high temperature which increases the blister volume and reduces G in turn. Various unaccountable factors as stated in the introduction section could also be the explanation.

DISCUSSION AND CONCLUSION

We have shown how a blister delamination can be driven by thermal expansion of an internal working gas using a TMA, and how the interface energy of a thin polymer film adhered onto a rigid substrate can be measured. The new method provides an easy adhesion test which is virtually identical to the notorious failure mode in coating delamination.

The stability of the thermal blister delamination in this paper is, in many respects, similar to a fixed-grip configuration in fracture mechanics, in that G is constrained and there is a maximum extent to which the crack can grow at a fixed temperature. This is in sharp contrast to the constant pressure or fixed load mode, where instability sets in once the crack-driving force exceeds a threshold. In predicting the life-span of most engineering parts, G in a stable crack propagation is as important as G in initiation. The constant working gas mass blister test in this paper proves to be a viable method to measure both strain release rates in one specimen.

The case where $p_0 = 0$ and $V_0 = 0$ is of particular interest in thin film delamination. From Eq. (10b), A (or a) is shown to depend solely on W and nRT, but *not* on the mechanical properties such as E and film dimension h. Provided the adhesive strength (W) remains a constant interface parameter independent of temperature, improvement of the flexural strength of stiffness of the polymer will *not* reduce the degree of damage. This is reminiscent of the lenticular cracks in thin ceramic films under a pure bending mode, where energy balance required $A = (\beta/W)nRT$ with β a numerical constant [23]. On the other hand, the extent of blistering in the vertical direction (y_0) at equilibrium relies

predominantly on the temperature-dependent mechanical properties. In a blister test, W can therefore be determined by the lateral dimension a alone, and E by the vertical dimension y_0.

One application of the present work is the "popcorn" cracking in many plastics electronics packages [1]. Moisture diffusing through the

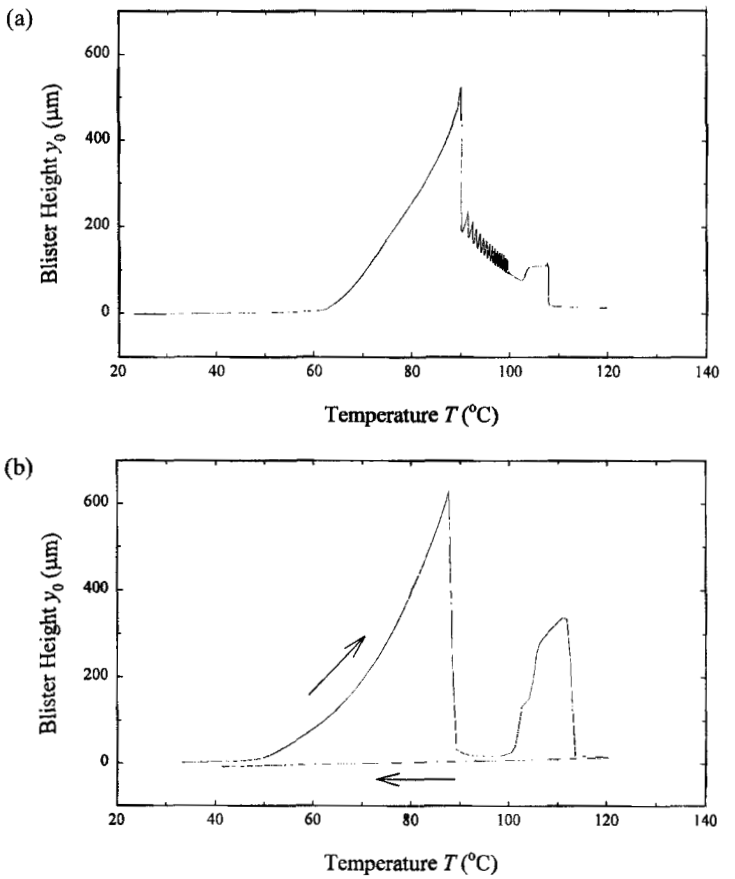

FIGURE 7 Two typical sets of data showing leak of working gas a debonding area grows beyond the specimen width. The measured y_0 followed a pure thermal expansion of aluminium before the *TMA* probe was lifted up by the internal pressure. In both cases, gas leaked at about 90°C. (a) An intermittent leakage caused a series of wriggles of y_0 as T increases. (b) A small droplet of water was introduced in the dead volume before heating. Water evaporation at temperature close to 100°C led to a second delamination. Subsequent cooling showed thermal contraction of aluminium substrate, α_{Al}.

encapsulant and the subsequent accumulation at the interface serves as the initial working gas to create a blister crack. As the part is subjected to solder to reflow at over 200°C, or temperature cycling, the expanding gas causes a blister delamination to propagate at the polymer/substrate interface reaching the edge of a lead frame. Increase in tensile stress on the surface defects and flaws as a result of the blister bulging eventually drives a major crack running through the coating. Hot gas leaks out like a "popcorn". A similar phenomenon was observed in two of our experiments (Figs. 7a and 7b), In Figure 7a, a delamination reached the edge of a specimen releasing a small amount of working gas intermittently over a period of time. The oscillations of the blister height is the result of the alternating leak and seal. In Figure 7b, small droplets of water were introduced into the drilled bore in the substrate before the polymer film was adhered. As the delamination grew beyond the specimen width, a small amount of air/moisture mixture leaked. The weighted *TMA* probe then slammed onto the substrate at 87°C and the film was re-adhered to the substrate. At 100°C, water evaporated and caused a second delamination process. The expanding moisture eventually leaked out of the bore at 113°C and the *TMA* probe was again in contact with the substrate. The $y_0(T)$ measurement during subsequent cooling corresponds to α_{Al}.

Acknowledgements

The authors are grateful to A/Prof. Yue Chee Yoon of the Department of Mechanical and Production Engineering of Nanyang Technological University (Singapore) and Dr. Stephen Osiyemi of Gintic Institute of Manufacturing Technology for invaluable discussions, and Ms. Zhang Weihong of Gintic for technical assistance.

References

[1] Lau, J. H., *Thermal stress and strain in microelectronics packaging* (Van Nostrand Reinhold, NY, 1993).
[2] Matienzo, L. J. and Egitto, F. D., *Solid State Tech.* **7**, 99 (1995).
[3] Thouless, M. D. and Jensen, H. M., *J. Adhesion* **38**, 185 (1992).
[4] Williams, M. L., *J. Appl. Polym. Sci.* **13**, 29 (1969).
[5] Hinkley, J. A., *J. Adhesion* **16**, 115 (1983).
[6] Gent, A. N. and Lewandowski, L. H., *J. Appl. Polym. Sci.* **33**, 1567 (1987).

[7] Fernando, M. and Kinloch, A. J., *Int. J. Adhesion Adhesives* **10**, 69 (1990).
[8] Briscoe, B. J. and Panesar, S. S., *Proc. R. Soc. Lond. A* **433**, 23 (1991).
[9] Chu, Y. Z. and Durning, C. J., *J. Appl. Polym. Sci.* **45**, 1151 (1992).
[10] Malyshev, B. M. and Salganik, R. L., *Int. J. of Fracture Mechanics* **1**, 114 (1965).
[11] Wan, K.-T. and Mai, Y.-W., *Int. J. Fracture* **74**, 181 (1995).
[12] Allen, M. G. and Senturia, S. D., *J. Adhesion* **25**, 303 (1988).
[13] Allen, M. G. and Senturia, S. D., *J. Adhesion* **29**, 219 (1989).
[14] Dillard, D. A. and Bao, Y., *J. Adhesion* **33**, 253 (1991).
[15] Chang, Y.-S., Lai, Y.-H. and Dillard, D. A., *J. Adhesion* **27**, 197 (1989).
[16] Lai, Y.-H. and Dillard, D. A., *J. Adhesion* **31**, 177 (1990).
[17] Lai, Y.-H. and Dillard, D. A., *J. Adhesion* **33**, 63 (1990).
[18] Wan, K.-T. and Mai, Y.-W., *Acta Metall. Mater.* **43**, 4109 (1995).
[19] Hencky, H., *Math. Phys.* **63**, 311 (1915).
[20] Williams, J. G., *Fracture Mechanics of Polymers* (John Wiley and Sons, NY, 1984).
[21] Williams, J. G., *Int. J. Fracture*, to be published in 1997.
[22] Wan, K.-T., in preparation.
[23] Wan, K.-T., Horn, R. G., Courmont, S. and Lawn, B. R., *J. Mater. Res.* **8**, 1128 (1993).